Non-FSI 3D Hemodynamic Simulations in Time-Dependent Domains

Y. V. Vassilevski, O. N. Bogdanov, X. V. Chesnokova, A. A. Danilov, T. K. Dobroserdova, D. D. Dobrovolsky, and A. V. Lozovskiy

1 Introduction

Computational analysis of functionality of the cardiovascular system is based on equations describing incompressible fluid flows. Blood flows interact inevitably with surrounding elastic tissues. The most general approach to hemodynamic simulations is the solution of fluid–structure interaction (FSI) problems [1–4]. The numerical solution of 3D FSI problems is computationally expensive, is time-consuming, and requires usage of parallel computers. In addition, FSI simulations are hard to personalize since elastic properties of vessels cannot be retrieved in vivo with appropriate accuracy. To overcome these difficulties, reduced hemodynamic models have been developed in the last few decades [5, 6]. The reduced models, however, cannot represent 3D flows and thus cannot provide important characteristics such as vorticity, wall shear stress, etc.

Several applications allow us to simulate 3D blood flows with less computational cost than the numerical solution of the 3D FSI problems. In this paper we address two such applications: blood flow in the left ventricle of a patient, and blood flow in the aortic bifurcation. In the first case the input data is dynamic ceCT medical images [7]; in the second case the input corresponds to a benchmark [8]. We consider mathematical formulations which can replace FSI formulations and still

Y. V. Vassilevski (✉) · A. A. Danilov
Marchuk Institute of Numerical Mathematics RAS, Moscow, Russia

Sechenov University, Moscow, Russia

O. N. Bogdanov · X. V. Chesnokova · D. D. Dobrovolsky
Sechenov University, Moscow, Russia

T. K. Dobroserdova · A. V. Lozovskiy
Marchuk Institute of Numerical Mathematics RAS, Moscow, Russia

R. P. Mondaini (ed.), *Trends in Biomathematics: Chaos and Control in Epidemics, Ecosystems, and Cells*, https://doi.org/10.1007/978-3-030-73241-7_16

provide feasible 3D solutions. For theoretical study and numerical details we refer to [1, 7, 9] for the first application and [8, 10] for the second application.

The paper is organized as follows. In Sect. 2 we pose the 3D FSI problem in a monolithic setting. In Sect. 3 we discuss the incompressible Navier–Stokes equations for flows in a time-dependent domain whose walls are moving (e.g. heart ventricles). In Sect. 4 we introduce a multiscale model for blood flows in the aortic bifurcation and compare it with the reference FSI solution.

2 Fluid–Structure Interaction

In the fluid–structure interaction setting, a time-dependent domain $\Omega(t) \subset \mathbb{R}^3$ is partitioned into fluid subdomain $\Omega^f(t)$ and structure subdomain $\Omega^s(t)$ with interface $\Gamma^{fs}(t) := \partial\Omega^f(t) \cap \partial\Omega^s(t)$ where the fluid–structure interaction occurs. The reference domains

$$\Omega_f = \Omega^f(0), \quad \Omega_s = \Omega^s(0)$$

are mapped by a deformation

$$\boldsymbol{\xi}^s : \Omega_s \times [0,t] \to \bigcup_{t\in[0,T]} \Omega^s(t), \quad \boldsymbol{\xi}^f : \Omega_f \times [0,t] \to \bigcup_{t\in[0,T]} \Omega^f(t).$$

For the structure, the deformation is naturally related to the displacement $\mathbf{u}^s$ via $\mathbf{u}^s(\mathbf{x},t) := \boldsymbol{\xi}^s(\mathbf{x},t) - \mathbf{x}$ and velocity $\mathbf{v}^s := \partial_t \mathbf{u}^s = \partial_t \boldsymbol{\xi}^s(\mathbf{x},t)$. For the fluid, the deformation is artificial and is defined by a continuous extension $\mathbf{u}^f := \mathrm{Ext}(\mathbf{u}^s)$ of the displacement field $\mathbf{u}^s$ to Ω_f:

$$\boldsymbol{\xi}^f(\mathbf{x},t) = \mathbf{u}^f + \mathbf{x} \quad \text{in } \Omega_f \times [0,t], \quad \boldsymbol{\xi}^f = \boldsymbol{\xi}^s \quad \text{on } \Gamma_{fs} \times [0,t],$$

where $\Gamma_{fs} := \Gamma^{fs}(0)$. There exist methods providing a mapping $\boldsymbol{\xi}^f$ [1]. Of course, $\boldsymbol{\xi}^f$ is not Lagrangian since it does not follow fluid particles trajectories.

In contrast to equations for the structure, equations for the fluid deal with the velocity vector field $\mathbf{v}^f$ and the pressure scalar field p^f given in the current domain $\Omega^f(t)$ for $t \in [0,T]$. We set $p^s = 0$ in Ω_s and define the global pressure variable $p = p^{f,s}$. For simplicity, we shall exploit the notations in the current configuration as $\mathbf{v}^f(\mathbf{x},t) := \mathbf{v}^f(\boldsymbol{\xi}^f(\mathbf{x},t),t)$, $p^f(\mathbf{x},t) := p^f(\boldsymbol{\xi}^f(\mathbf{x},t),t)$.

The monolithic approach [11] sets equations for displacements $\mathbf{u} = \mathbf{u}^{f,s}$ and velocities $\mathbf{v} = \mathbf{v}^{f,s}$ both in Ω^f and Ω^s. The globally defined deformation gradient $\mathbb{F} = \mathbb{I} + \nabla\mathbf{u}$ and its Jacobian $J := \det(\mathbb{F})$ contribute to each dynamic equation in the monolithic method:

$$\frac{\partial \mathbf{v}}{\partial t} = \begin{cases} \rho_s^{-1}\mathrm{div}\,(J(\boldsymbol{\sigma}_s \circ \boldsymbol{\xi}^s)\mathbb{F}^{-T}) & \text{in } \Omega_s, \\ (J\rho_f)^{-1}\mathrm{div}\,(J(\boldsymbol{\sigma}_f \circ \boldsymbol{\xi}^f)\mathbb{F}^{-T}) - (\nabla \mathbf{v})\left(\mathbb{F}^{-1}\left(\mathbf{v} - \dfrac{\partial \mathbf{u}}{\partial t}\right)\right) & \text{in } \Omega_f. \end{cases} \tag{1}$$

Here ρ_s and ρ_f are the solid and fluid densities, and $\boldsymbol{\sigma}_s$ and $\boldsymbol{\sigma}_f$ are the Cauchy stress tensors. Note that the dynamics of structure is given in the Lagrangian coordinates, whereas the dynamics of fluid is given in the Arbitrary Lagrangian–Eulerian framework. The kinematic equation in the structure

$$\frac{\partial \mathbf{u}}{\partial t} = \mathbf{v} \quad \text{in } \Omega_s \tag{2}$$

and incompressibility constraint in the fluid

$$\mathrm{div}\,(J\mathbb{F}^{-1}\mathbf{v}) = 0 \quad \text{in } \Omega_f \tag{3}$$

complete the system of the monolithic approach equations.

The above equations are complemented with initial conditions

$$\mathbf{u}(\mathbf{x}, 0) = \mathbf{0}, \quad \mathbf{v}(\mathbf{x}, 0) = \mathbf{v}_0(\mathbf{x}) \ \text{ in } \Omega(0) \tag{4}$$

and appropriate boundary conditions on the outer boundary. On the fluid–structure interface no-slip no-penetration of fluid and the balance of normal stresses are imposed

$$\mathbf{v}^s = \mathbf{v}^f \quad \text{and} \quad \boldsymbol{\sigma}_f \mathbb{F}^{-T}\mathbf{n} = \boldsymbol{\sigma}_s \mathbb{F}^{-T}\mathbf{n} \quad \text{on } \Gamma_{fs}, \tag{5}$$

where $\mathbf{n}$ is the unit normal vector on Γ_{fs}.

The solution of the FSI problem implies finding pressure p in fluid and continuous velocity and displacement fields $\mathbf{v}$, $\mathbf{u}$ in $\bar{\Omega}_f \cup \bar{\Omega}_s$ satisfying the set of Eqs. (1)–(5) and the boundary conditions. It is assumed that an extension rule $\mathbf{u}^f := \mathrm{Ext}(\mathbf{u}^s)$ is given.

It remains to define the Cauchy tensors for the fluid and the structure. They depend on chosen rheological model. For instance, for Newtonian fluid with viscosity μ_f

$$\boldsymbol{\sigma}_f = -p_f\mathbb{I} + \mu_f(\nabla \mathbf{v}\mathbb{F}^{-1} + \mathbb{F}^{-T}(\nabla \mathbf{v})^T) \tag{6}$$

and for Saint Venant–Kirchhoff material of the structure with Lame constants λ_s, μ_s

$$\boldsymbol{\sigma}_s = \frac{1}{J}\mathbb{F}(\lambda_s \mathrm{tr}(\mathbb{E})\mathbb{I} + 2\mu_s\mathbb{E})\mathbb{F}^T, \tag{7}$$

where $\mathbb{E} = \frac{1}{2}\left(\mathbb{F}^T\mathbb{F} - \mathbb{I}\right)$ is the Lagrange–Green strain tensor.

The common approach to the solution of the FSI problem in domains with complex geometry is the finite element method on unstructured tetrahedral meshes since these meshes can be generated in any domain, and may be locally refined. Fractional time stepping is computationally cheaper than implicit schemes, but imposes restrictions on the time step. Implicit and semi-implicit schemes may afford large time steps [1, 11–13]. In any case, the solution of a 3D FSI problem is computationally expensive: passing 3D benchmarks may require hundreds and thousands of core-hours. Moreover, patient-specific simulations require personalized elastic models of wall tissues which cannot be retrieved in clinical practice.

3 Navier–Stokes Equations in Time-Dependent Domain

Let the computational domain contain only fluid and the mapping $\Omega(t) = \boldsymbol{\xi}(\Omega_0 \times \{t\})$ be given, the deformation gradient $\mathbb{F} = \nabla_{\mathbf{x}}\boldsymbol{\xi}$ and its Jacobian $J = \det(\mathbb{F})$ satisfy

$$\inf_Q J \geq c_J > 0, \quad \sup_Q(\|\mathbb{F}\|_F + \|\mathbb{F}^{-1}\|_F) \leq C_F, \quad \text{with } \|\mathbb{F}\|_F := \mathrm{tr}(\mathbb{F}\mathbb{F}^T)^{\frac{1}{2}}, \tag{8}$$

where $Q := \Omega_0 \times [0, T]$ denotes the space-time cylinder and C_F, c_J denote positive constants.

The dynamics of incompressible Newtonian fluid is described by the fluid subset of Eqs. (1)–(5) for velocity $\mathbf{v}$ and pressure p defined in Q

$$\begin{cases} \dfrac{\partial \mathbf{v}}{\partial t} - (J\rho_f)^{-1}\mathrm{div}\,(J(\boldsymbol{\sigma}_f \circ \boldsymbol{\xi})\mathbb{F}^{-T}) + (\nabla \mathbf{v})\left(\mathbb{F}^{-1}\left(\mathbf{v} - \dfrac{\partial \boldsymbol{\xi}}{\partial t}\right)\right) = \mathbf{f} \\ \mathrm{div}\,(J\mathbb{F}^{-1}\mathbf{v}) = 0 \end{cases} \quad \text{in } Q, \tag{9}$$

with body forces $\mathbf{f}$ (e.g. gravity) and the initial condition $\mathbf{v}(\mathbf{x}, 0) = \mathbf{v}_0(\mathbf{x})$ in Ω_0. The fluid is assumed to be Newtonian (6) although a nonlinear rheological law is also applicable.

The boundary conditions depend on physical characteristics of boundary parts: on the wall part one imposes no-penetration no-slip or slip condition for velocity, on the inlet/outlet one may impose the free flow condition involving the Cauchy tensor; for details we refer to [1, 9].

An approximate solution of (9) may be obtained by the finite element method on a tetrahedral mesh in Ω_0. A popular choice is P2-P1 Taylor–Hood elements (piecewise quadratic continuous velocities and piecewise linear continuous pressures). According to the stability and convergence analysis [9], the Taylor–Hood elements and the backward Euler discretization in time (with linearized inertia term) provide the optimal error bound $O(\max\{h^2; \Delta t\})$ under feasible assumptions. The error norm is the same for the stability and the convergence estimates and is typical for the numerical analysis of the finite element solution of the Navier–Stokes equations.

The time step Δt is not limited by the CFL restriction. The second order in time approximation can be achieved by using the second order backward differences in time instead of the backward Euler time stepping. Numerical tests confirm the second order (in space) convergence of the Taylor–Hood solution to an analytical solution [9].

In practice, the mapping $\boldsymbol{\xi}$ may be defined by a sequence of topologically invariant meshes which differ only in nodes positions. The first mesh in the sequence is referred to as the reference mesh at time $t = 0$ with reference mesh nodes. Let $\boldsymbol{\xi}(\mathbf{x}, t_k)$ be the position of a reference mesh node with position $\mathbf{x}$ at time $t = t_k$. We define the mapping $\boldsymbol{\xi}^k$ as the continuous piecewise linear vector function with values $\boldsymbol{\xi}(\mathbf{x}, t)$ at mesh nodes for $t = t_k$, and define the function $\boldsymbol{\xi}(\mathbf{x}, t)$ as the linear interpolation between mappings $\boldsymbol{\xi}^{k-1}$ and $\boldsymbol{\xi}^k$ for $t_{k-1} < t < t_k$. Such continuous in space and time piecewise linear in mesh cells and time intervals mapping is an approximation of an unknown smooth mapping $\boldsymbol{\xi}$ contributing an additional modelling error. However, this error is small and does not pollute the solution essentially. The approach was successfully applied to simulation of 3D blood flow in the left ventricle of a patient [1, 7]. Figure 1 demonstrates the computational tetrahedral mesh and computed blood velocities at two instants of the systole.

If the mapping $\boldsymbol{\xi}$ is reconstructed from medical images, no-penetration no-slip condition requires both normal and tangential components of the wall velocity. The normal velocity may be recovered from any dynamic sequence of medical images by $v_\Gamma = \mathbf{n} \cdot (\boldsymbol{\xi}_t \circ \boldsymbol{\xi}^{-1})$, whereas the tangential velocity needs special treatment of the images, e.g. speckle tracking.

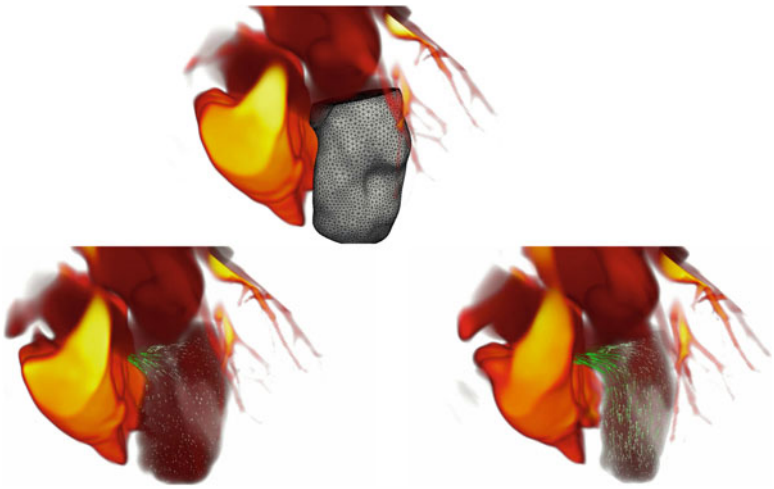

Fig. 1 Computational mesh for the left ventricle (top), blood velocities at two instants of the systole (bottom left, bottom right)

4 Multiscale Hemodynamic Model in Compliant Bifurcations

It is known [14] that pulsatile flows in vessels with rigid and compliant walls differs considerably. One cannot use the solution of the Navier–Stokes equations as an approximation to the solution of the FSI problem: flow rates and pressures are essentially different even for a straight tube. However, in case of compliant vessel bifurcation, one can use the Navier–Stokes equations in a domain with a rigid wall provided that the domain is a vicinity of the bifurcation and the 3D Navier–Stokes equations are coupled to 1D and 0D reduced hemodynamic models in a multiscale hemodynamic model [10].

The 3D Navier–Stokes equations in a short bifurcation domain Ω with rigid walls are reduced to

$$\begin{cases} \dfrac{\partial \mathbf{v}}{\partial t} - \rho_f^{-1} \operatorname{div} \boldsymbol{\sigma}_f + (\nabla \mathbf{v})\mathbf{v} = \mathbf{f} \\ \operatorname{div} \mathbf{v} = 0 \end{cases} \quad \text{in } \Omega, \tag{10}$$

with the initial condition $\mathbf{v}(\mathbf{x}, 0) = \mathbf{v}_0(\mathbf{x})$, no-slip boundary condition on the rigid wall, and interface boundary conditions on the inlet and two outlets. The latter conditions couple (10) with a 0D hydraulic model of an absorber which mimics an elastic sphere $\Omega_{0\mathrm{D}}$ filled with fluid. The parameters of the absorber model are volume $V(t)$ and variable $p_{0\mathrm{D}}(t)$ denoting the difference between fluid and external pressures. The kinematic equation for the elastic sphere filled with fluid is

$$I \frac{d^2 V}{dt^2} + R_0 \frac{dV}{dt} + \frac{V - V_0}{C} = p_{0\mathrm{D}}, \tag{11}$$

where V_0 is the volume at rest under $p_{0\mathrm{D}} = 0$; I, C, R_0 are inertia, expansibility, and resistance parameters of the sphere. The 0D absorber model mimics the compliance of the original compliant 3D bifurcation and interfaces the 3D Navier–Stokes equations in rigid walls from one side and 1D hemodynamic equations in the branches of the bifurcation, from the other side.

The 1D equations represent a reduced model for pulsatile flow in tubes with elastic walls. They are able to reproduce the pulse wave propagation under assumption of small ratio of tube diameter to its length. These equations stem from the mass and momentum conservation laws:

$$\partial A/\partial t + \partial (A\overline{v})/\partial x = 0, \tag{12}$$

$$\partial \overline{v}/\partial t + \partial \left(\overline{v}^2/2 + \overline{p}/\rho_b \right)/\partial x = f_{\overline{v}}, \tag{13}$$

where x is the coordinate along the tube, $A(t, x)$ is the cross-section area of the tube, $\overline{v}(t, x)$ and $\overline{p}$ are the averaged over the cross-section linear velocity and fluid pressure, ρ_b is the fluid density, $f_{\overline{v}} = -2(n+2)\mu_b \pi \overline{v} A^{-1} \rho_b^{-1}$ is the flow

deceleration friction term. The latter term is derived under assumption of the axisymmetric velocity profile [8]. The third equation of the 1D reduced model incorporates elastic properties of the tube wall via pressure to cross-section area relationship $p(A)$

$$\overline{p} = p_d + \beta A_d^{-1}(\sqrt{A} - \sqrt{A_d}), \qquad \beta = 4\sqrt{\pi}Eh/3, \tag{14}$$

where A_d is the diastolic cross-sectional area, $p_d = 9.5$ kPa is the diastolic pressure, E and h are the Young's modulus and thickness of the wall, respectively. For a review of different variants of (14) we refer to [6, 15].

The coupling equations at the 1D-0D and 3D-0D interfaces are

$$\begin{array}{ll} \frac{dV}{dt} = Q_{1\mathrm{D}} - Q_{3\mathrm{D}}, & \text{conservation of mass} \\ \overline{p} - p_{0\mathrm{D}} = R_{1\mathrm{DOD}} Q_{1\mathrm{D}}, & \text{Poiseuille law} \\ p_{0\mathrm{D}} - \overline{p} = R_{0\mathrm{D3D}} Q_{3\mathrm{D}}, & \text{Poiseuille law} \end{array} \tag{15}$$

where $Q_{1\mathrm{D}} = A\overline{v}$ is the 1D fluid flux, $Q_{3\mathrm{D}} = -\int_\Gamma \mathbf{v} \cdot \mathbf{n} ds$ is the 3D fluid flux through inlet/outlet from Ω_{0D} to Ω_{3D}, $R_{1\mathrm{D0D}}$ and $R_{0\mathrm{D3D}}$ are the resistance coefficients. Positive parameters R_0, $R_{1\mathrm{D0D}}$ and $R_{0\mathrm{D3D}}$ are shown to produce dissipation in the cumulative energy balance of the complete 1D–0D–3D system [16].

For numerical examination, we consider an idealized model of the aortic bifurcation [8]. The abdominal aorta is represented by the inlet cylinder Ω_a with length $L_a = 8.6$ cm, radius $r_a = 0.86$ cm, diastolic cross-sectional area $A_a = 1.8062\,\mathrm{cm}^2$, wall thickness $h_a = 1.032$ mm, Young's modulus $E_a = 500$ kPa, density $\rho_w = 1\,\mathrm{g/cm}^3$. The iliac arteries are represented by two equal outlet cylinders with length $L_i = 8.5$ cm, radius $r_i = 0.60$cm, diastolic cross-sectional area $A_i = 0.9479\,\mathrm{cm}^2$, wall thickness $h_i = 0.72$ mm, Young's modulus $E_i = 700$ kPa, and the same density $\rho_w = 1\,\mathrm{g/cm}^3$. The blood with viscosity $\mu_b = 4$ mPa s, density $\rho_b = 1060\,\mathrm{kg/m}^3$, mean flow rate $\bar{Q}_a = 0.4791$ l/min, and pulsatile velocity profile at the inlet $v(\xi, t) = \overline{v}(t)n^{-1}(n+2)[1 - (\xi r^{-1})^n]$, where r is the lumen radius, ξ is the radial coordinate, $n = 9$ is the polynomial order providing a good approximation of experimentally measured profile, $\overline{v}(t)$ is a given axial blood flow velocity averaged over the cross-section [8]. Each iliac cylinder is coupled with a three-element 0D Windkessel model [10].

The numerical solution of the 1D equation is based on the grid-characteristic method [1, 17, 18]. The numerical solution of the 3D Navier–Stokes equations is based on the P2-P1 Taylor–Hood finite elements and the backward Euler discretization in time (with linearized inertia term) on a tetrahedral mesh in bifurcation domain Ω. Coupling between the 1D,0D,3D models is achieved via iterations for (15) at the interfaces.

Table 1 presents the average relative error $avg\%$ and the maximum relative error $max\%$ for the flux and the pressure. The reference solution is provided by the 3D

Table 1 Error at the iliac arteries junction: flow rate and pressure computed by the numerical solutions of the Navier–Stokes equations in rigid walls and the multiscale method

	Flux		Pressure	
Error in method	avg%	max%	avg%	max%
NSE with rigid walls	9.15	30.02	1.41	8.31
Multiscale	1.15	4.49	2.02	3.48

FSI equations. The error produced by the Navier–Stokes equations in rigid walls is prohibitively large.

Acknowledgments The work has been supported by the Russian Science Foundation grant 19-71-10094.

References

1. Yu. Vassilevski et al. *Personalized Computational Hemodynamics: Models, Methods, and Applications for Vascular Surgery and Antitumor Therapy*, Academic Press (2020).
2. G. Kassab. *Coronary Circulation: Anatomy, Mechanical Properties, and Biomechanics*, Springer International Publishing (2019).
3. M. Labrosse, Ed. *Cardiovascular mechanics*, Taylor & Francis Group (2019).
4. A. Quarteroni et al. *Mathematical Modelling of the Human Cardiovascular System: Data, Numerical Approximation, Clinical Applications*, Cambridge University Press (2019).
5. Y. Shi, P. Lawford, R. Hose, Review of zero-D and 1D models of blood flow in the cardiovascular system. *Biomed. Eng. Online* **10**(33) (2011).
6. N. Bessonov et al., Methods of blood flow modelling. *Math. Model. Nat. Phenom.* **11** (1) (2016).
7. A. Danilov et al., A finite element method for the Navier-Stokes equations in moving domain with application to hemodynamics of the left ventricle. *Russian J. Numer. Anal. Math. Modelling* **32**(4) (2017).
8. N. Xiao, J. Alastruey-Arimon, C.A. Figueroa, A systematic comparison between 1D and 3D hemodynamics in compliant arterial models. *Int. J. Numer. Methods Biomed. Eng.* **30** (2) (2014).
9. A. Lozovskiy, M. Olshanskii, Y. Vassilevski, A quasi-Lagrangian finite element method for the Navier-Stokes equations in a time-dependent domain. *Comput. Methods Appl. Mech. Engrg.* **333** (2018).
10. T. Dobroserdova et al., Multiscale models of blood flow in the compliant aortic bifurcation. *Appl. Math. Lett.* **93**C (2019).
11. J. Hron and S. Turek. *A Monolithic FEM/multigrid Solver for an ALE Formulation of Fluid-Structure Interaction with Applications in Biomechanics*, Springer Berlin Heidelberg (2006).
12. A. Lozovskiy et al., An unconditionally stable semi-implicit FSI finite element method. *Comput.Methods Appl.Mech.Engrg.* **297** (2015).
13. A. Lozovskiy, M. Olshanskii, Y. Vassilevski, Analysis and assessment of a monolithic FSI finite element method. *Computers and Fluids*, **179** (2019).
14. C. Caro et al. *The Mechanics of the Circulation*, second ed. Cambridge University Press (2012).
15. Yu. Vassilevski, V. Salamatova and S. Simakov, On the elasticity of blood vessels in one-dimensional problems of hemodynamics. *J. Computational Mathematics and Mathematical Physics* **55**(9) (2015).

16. T. Dobroserdova, M. Olshanskii and S. Simakov, Multiscale coupling of compliant and rigid walls blood flow models. *Int. J. Numer. Methods In Fluids* **82** (12) (2016).
17. A. Kholodov, Some dynamical models of multi-dimensional problems of respiratory and circulatory systems including their interaction and matter transport. In: *Computer Models and Medicine Progress*, Nauka, Moskva (2001).
18. K. Magomedov and A. Kholodov, *Grid-Characteristics Numerical Methods*, second ed. Urait, Moscow (2018).